A CENTRAL WENO-TVD SCHEME FOR HYPERBOLIC CONSERVATION LAWS

Yousef Hashem Zahran[1]

Abstract. The purpose of this paper is to carry out a modification of the finite volume WENO (weighted essentially non-oscillatory) scheme of Titarev and Toro [10]. This modification is done by using the third order TVD flux [10] as building blocks in spatially fifth order WENO schemes, instead of the second order TVD flux proposed by Titarev and Toro. The resulting scheme improves both the original and Toros flux in terms of order of accuracy, convergence and better resolution of discontinuities. The numerical solution is advanced in time by TVD Runge-Kutta method. Extension to systems is carried out by the component-wise application of the scalar framework. Numerical experiments confirm the high resolution of the proposed scheme. Thus, a considerable amount of simplicity and robustness is gained while retaining the expected third-order resolution.

AMS Mathematics Subject Classification (2000): 65M10, 65M05

Key words and phrases: WENO, Runge-Kutta methods, TVD schemes, conservation laws, semi-discrete finite volume, Euler equations, Burger equation.

1. Introduction

We are concerned with improved high-accuracy methods for solving hyperbolic conservation laws. Hyperbolic conservation laws arise in area as diverse as compressible gas dynamics, shallow water equations, weather prediction, and many others. Analytical solutions are available only in a very few special cases and numerical methods must be used in practical applications.

There are essentially two types of such methods, namely upwind schemes and central schemes.

The prototype of upwind schemes is the first-order Godunov scheme in which a piecewise constant interpolant is evolved exactly to the next time step according to the conservation law. This evolution involves a solution of Riemann problems on the boundaries of each cell, which is interpreted as an up-winding procedure, as one has to differ between left-going and right-going waves in order to compute the flux in these non-smooth regions.

A general procedure used to obtain high accuracy in space with upwind schemes is based on a high-order reconstruction of the field variables. This is obtained by approximating the field at a given time by a piecewise polynomial rather than by a piecewise constant. Generally, a piecewise reconstruction of

---

[1]Physics and Mathematics Department, Faculty of Engineering, Port Said, Egypt
e-mail: yousef_hashem_zahran@yahoo.com

degree r should guarantee spatial accuracy of order (r+1) for a smooth solution. Since the drawback of a high order reconstruction is the oscillations it might create, several methods were suggested to combine the up-winding framework with a mechanism to prevent the creation and evolution of such spurious numerical oscillations. In particular, a class of Essentially Non-Oscillatory (ENO) schemes was presented in [4]. The key idea in the r-th order ENO reconstruction procedure used in [4] is to consider r possible stencils covering the given cell and select only one, the smoothest, stencil. The reconstruction polynomial is then built using this selected stencil.

The Weighted Essentially Non-Oscillatory (WENO) reconstruction [5] takes a convex combination of all r stencils with nonlinear solution adaptive weights. The design of the weights involves local estimates of the smoothness of the solution in each possible stencil so that the reconstruction achieves (2r-1)-th order spatial accuracy in smooth regions and emulates the r-th order ENO reconstruction near discontinuities.

Central schemes, on the other hand, do not explicitly use the wave propagation information. This makes them very simple, efficient and applicable to problems where the Riemann solution is not known or is too costly to be used. The Lax-Friedrichs (LxF) scheme is the best known first-order central scheme. It is the forerunner for such central schemes and is based on piecewise constant reconstructions.

The accuracy of the schemes can be increased by using higher reconstructions. Nessyahu-Tadmor introduced in [7] a second-order extension (NT) along these lines, using the piecewise linear MUSCL reconstructions. Liu and Tadmor [6] introduced a third-order central scheme by using the piecewise quadratic MUSCL reconstructions with the same framework of NT scheme. Harten [3] introduced the notion of second-order TVD schemes. TVD schemes avoid spurious oscillations by reverting to first-order of accuracy near discontinuities and extrema and therefore unsuitable for the applications involving large time evolution of complex structures.

A central third-order TVD scheme has been presented in [13]. It has been shown that the scheme is TVD and gives good numerical results both on scalar equations and on the Euler equations.

In this paper, we combine the upwind and central approaches to obtain a new scheme, which enjoys the desired properties of both approaches; the central framework provides the robustness and the simplicity while the WENO reconstruction provides the required high-order, non-oscillatory reconstruction.

In the above-mentioned methods, it is noticed that the only lower order (first order) fluxes are used as the building block in high order schemes.

In this paper we used the third order TVD flux [13], instead of Toro second order TVD flux [10], as a building block in spatially fifth-order WENO reconstruction as the building block in higher methods (WENO) with TVD Runge-Kutta time stepping. Compared to the original WENO (using first-order flux) and with the second-order TVD flux [10], the new fluxes improve both the original and Toros flux in terms of the order of accuracy, convergence and better resolution of discontinuities. Numerical results suggest that the new scheme is

superior to the original TVD and WENO schemes, in terms of better convergence, higher overall accuracy and better resolution of discontinuities. This is especially evident for long-time evolution problems containing both smooth and non-smooth features.

The paper is organized as follows. In section 2 we briefly review the WENO reconstruction and the TVD Runge-Kutta method for time discretization. In section 3 we review the fluxes to be used as the building block in the numerical methods, including the third-order TVD flux [13]. The resulting method is described in section 4, for both scalar and systems cases. Finally, several examples can be found in section 5. These numerical examples clearly demonstrate the accuracy, non-oscillatory and robustness properties of our scheme.

2. Numerical Methods

We are concerned with the approximations of scalar hyperbolic conservation law

$$(2.1a) \qquad u_t + f(u)_x = 0, \quad -\infty < x < \infty, \quad t \geq 0$$

subjected to the initial condition

$$(2.1b) \qquad u(x,0) = u_0(x)$$

To approximate solution of (2.1) we discretize both space and time assuming uniform mesh spacing Δx and Δt respectively. We denote the spatial grid points by $x_j = j\Delta x$ and the time steps by $t^n = n\Delta t$. Here and below $\lambda = \Delta t/\Delta x$ denotes the usual fixed-mesh ratio. Since the solutions of (2.1) can develop discontinuities (shocks), even for smooth initial data, the quantities that will be used on the discrete level are cell-averages. The numerical approximation of the cell average in the cell $I_j = [x_{j-\frac{1}{2}}, x_{j+\frac{1}{2}}]$ centered around x_j at time t^n, is denoted by u_j^n:

$$(2.2) \qquad u_j^n = \frac{1}{\Delta x} \int_{x_{j-\frac{1}{2}}}^{x_{j+\frac{1}{2}}} u(x,t^n)dx$$

Assuming that the cell averages at time t^n, u_j^n are known, our goal is to compute the cell averages at the next time step t^{n+1}.

First, from u_j^n, we reconstruct the point values of the function $u(x,t^n)$ via a suitable nonlinear piecewise polynomial interpolation $P_j(x)$, $x \in I_j$, taking into account conservation, accuracy and non-oscillatory requirements, for each cell I_j. The reconstruction we use is WENO [5]. We will describe our implementation of the reconstruction step in section (2.1) for completeness. As a result, at each cell interface $x_{j\pm\frac{1}{2}}$ the reconstruction produces two different values of the function $u(x)$, namely the left-extrapolated values and right-extrapolated value:

$$u_{j+\frac{1}{2}}^L = P_j(x_{j+\frac{1}{2}}), \quad u_{j+\frac{1}{2}}^R = P_{j+1}(x_{j+\frac{1}{2}}).$$

Note that, in general, $P(x)$ will have jump discontinuities at the points $x_{j\pm\frac{1}{2}}$. The evolution of the discontinuous data $u(x,t^n)$ can be computed by solving a sequence of generalized Riemann problems centred at $x_{j+\frac{1}{2}}$:

$$u_t + f(u)_x = 0, \quad t \geq t^n, \quad u(x,t^n) = \begin{cases} P_j(x), & x < x_{j+\frac{1}{2}} \\ P_{j+1}(x), & x > x_{j+\frac{1}{2}} \end{cases}$$

This is the framework of upwind methods.

On the other hand, in central schemes, the solution is updated by integrating (2.1) over I_j, we obtain the semi-discrete finite volume scheme

$$(2.3) \qquad \frac{d}{dt}(u_j(t)) = \frac{-1}{\Delta x}\left[f_{j+\frac{1}{2}} - f_{j-\frac{1}{2}} \right] = L_j(u)$$

where $u_j(t)$ is the space average of the solution in I_j at time t

$$(2.4) \qquad u_j(t) = \frac{1}{\Delta x} \int\limits_{x_{j-\frac{1}{2}}}^{x_{j+\frac{1}{2}}} u(x,t)dx$$

and $f_{j+\frac{1}{2}} = f(u(x_{j+\frac{1}{2}},t))$ is the numerical flux at $x_{j+\frac{1}{2}}$ and time t.

In the current ENO and WENO schemes the numerical solutions of (2.3) is advanced in time by means a TVD Runge-Kutta method [2] (see section (2.2)).

The numerical flux function at the cell boundaries $x_{j+\frac{1}{2}}$ is defined as a monotone function of left and right-extrapolated values $u^L_{j+\frac{1}{2}}, u^R_{j+\frac{1}{2}}$:

$$(2.5) \qquad f_{j+\frac{1}{2}} = f(u_{j+\frac{1}{2}},t) = f_{j+\frac{1}{2}}(u^L_{j+\frac{1}{2}}, u^R_{j+\frac{1}{2}}).$$

In the next subsection we will present the WENO reconstruction which supplies the required piecewise polynomial $P_j(x)$.

2.1. WENO Reconstruction

In this section we present the WENO reconstruction, which will be then utilized in section 4 to construct our new method.

As we know, the k-th order (in L^1 sense) ENO scheme chooses one smoothest stencil to reconstruct the value $u_{j+\frac{1}{2}}$ at the boundary $x_{j+\frac{1}{2}}$. Let us denote the k candidate stencils by

$$(2.6) \qquad S_r = \{x_{j-r}, \ldots, x_{j-r+k-1}\}, \qquad r = 0, \ldots, k-1.$$

If the stencil S_r happens to be chosen as the ENO interpolation stencil, then the k-th order ENO reconstruction of $u_{j+\frac{1}{2}}$ is

$$(2.7) \qquad P_j^{(r)}(x_{j+\frac{1}{2}}) = u_{j+\frac{1}{2}}^{(r)} = \sum_{i=0}^{k-1} C_{ri}u_{j-r+i}, \qquad r = 0, \ldots, k-1.$$

Here C_{ri} are constants coefficients given by [9].

$$(2.8) \qquad C_{ri} = \sum_{m=i+1}^{k} \frac{\displaystyle\sum_{\substack{\ell=0 \\ \ell \neq m}}^{k} \prod_{\substack{q=0 \\ q \neq \ell, m}}^{k} (r - q + 1)}{\displaystyle\prod_{\substack{\ell=0 \\ \ell \neq m}}^{k} (m - \ell)}.$$

For examples: for $k = 3$, $r = 1$

$$u_{j+\frac{1}{2}} = -\frac{1}{6}u_{j-1} + \frac{5}{6}u_j + \frac{1}{3}u_{j+1} + o(\Delta x)^3$$

and for $k = 3$, $r = 2$

$$u_{j+\frac{1}{2}} = \frac{1}{3}u_{j-1} - \frac{7}{6}u_j + \frac{11}{6}u_{j+1} + o(\Delta x)^3$$

To just use the one smoothest stencil among the k candidates for the approximation of $u_{j+\frac{1}{2}}$ is very desirable near discontinuities because it prohibits the usage of information on discontinuous stencils. However, it is not desirable in smooth regions because all the candidate stencils carry equally smooth information and thus can be used together to give a higher order (higher than r, the order of the base ENO schemes) approximation to $u_{j+\frac{1}{2}}$.

In [5] another approach for the reconstruction procedure has been suggested. There, in the so-called WENO reconstruction.

The basic idea is the following: instead of using only one of the candidate stencils to form the reconstruction, one can use a convex combination of all of them. To be more precise, one could assign a weight w_r to each candidate stencil S_r, $r = 0, 1, \ldots, k - 1$, and use these weights to combine the k different reconstructions to the value $u_{j+\frac{1}{2}}$ as

$$(2.9) \qquad P_j(x_{j+\frac{1}{2}}) = u_{j+\frac{1}{2}} = \sum_{r=0}^{k-1} w_r u_{j+\frac{1}{2}}^{(r)}$$

where $u_{j+\frac{1}{2}}^{(r)}$ is defined in (2.7). We require $w_r \geq 0$ and $\sum_{r=0}^{k-1} w_r = 1$ for consistency and stability.

If the function $u(x)$ is smooth in all the candidate stencils (2.6), there are constants d_r such that

$$(2.10) \qquad u_{j+\frac{1}{2}} = \sum_{r=0}^{k-1} d_r u_{j+\frac{1}{2}}^{(r)} = u(x_{j+\frac{1}{2}}) + o(\Delta x)^{2k-1}.$$

For example, d_r for $1 \leq k \leq 3$ are given by [5].

$d_0 = 1, k = 1$; $d_0 = 2/3, d_1 = 1/3, k = 2$; $d_0 = 3/10, d_1 = 6/10, d_2 = 1/10, k = 3$.

We can see that d_r is always positive and, due to consistency, $\sum_{r=0}^{k-1} d_r = 1$.

In this smooth case, we would like to have

$$(2.11) \qquad w_r = d_r + o(\Delta x)^{k-1}, \quad r = 0, 1, \ldots, k-1$$

which would imply the $(2k-1)$-th order accuracy

$$u_{j+\frac{1}{2}} = \sum_{r=0}^{k-1} w_r u_{j+\frac{1}{2}}^{(r)} = u(x_{j+\frac{1}{2}}) + o(\Delta x)^{2k-1}$$

When the function $u(x)$ has a discontinuity in one or more of the stencils (2.6), we would hope the corresponding weight (s) w_r to be essentially zero, to emulate the successful ENO idea.

Another consideration is that w_r should be smooth functions of the cell averages involved. Following the notations of [5], in order to guarantee convexity, the weights w_r are written as

$$(2.12a) \qquad w_r = \frac{\alpha_r}{\alpha_0 + \alpha_1 + \ldots + \alpha_{k-1}}, \quad r = 0, 1, \ldots, k-1,$$

where

$$(2.12b) \qquad \alpha_r = \frac{d_r}{(\varepsilon + \beta_r)^2}.$$

Here $\varepsilon > 0$ is introduced to avoid the denominator to become zero. We take $\varepsilon = 10^{-6}$ in our numerical tests. β_r are so called "smooth indicators" of the stencil S_r.

Several different ways to determine the smoothness indicator were suggested in [5], [9]. Here we use the measure taken from [5], which amounts to a measure on the L^2-norms of the derivatives:

$$(2.13) \qquad \beta_r = \sum_{\ell=1}^{k-1} \int_{x_{j-\frac{1}{2}}}^{x_{j+\frac{1}{2}}} (\Delta x)^{2\ell-1} (P_r^{(\ell)})^2 \, dx$$

where $P_r^{(\ell)}$ is the ℓ-th derivative of $P_r(x)$.

An explicit integration of (2.13) yields:

For $k = 2$,

$$(2.14) \qquad \beta_0 = (u_{j+1} - u_j)^2, \quad \beta_1 = (u_j - u_{j-1})^2$$

and for $k = 3$,

$$(2.15) \qquad \begin{aligned} \beta_0 &= \tfrac{13}{12}(u_j - 2u_{j+1} + u_{j+2})^2 + \tfrac{1}{4}(3u_j - 4u_{j+1} + u_{j+2})^2, \\ \beta_1 &= \tfrac{13}{12}(u_{j-1} - 2u_j + u_{j+1})^2 + \tfrac{1}{4}(u_{j-1} - u_{j+1})^2, \\ \beta_2 &= \tfrac{13}{12}(u_{j-2} - 2u_{j-1} + u_j)^2 + \tfrac{1}{4}(u_{j-2} - 4u_{j-1} + 3u_j)^2 \end{aligned}$$

This indicates that (2.14) gives third-order WENO scheme, and (2.15) gives a fifth-order one.

2.2. Time Discretization

Up to now we have only considered spatial discretizations, leaving the time variable continuous. In this section we consider the issue of time discretization. The time discretization will be implemented by a class of high-order TVD Runge-Kutta methods developed in [2].

These Runge-Kutta methods are used to solve a system of initial value of ordinary differential equations written as

$$(2.16) \qquad \frac{du}{dt} = L(u),$$

where $L(u)$ is an approximation to the derivative $(-f(u)_x)$ in the differential equation (2.1).

In [2], schemes up to third order were found to satisfy the TVD conditions. The optimal second-order TVD Runge-Kutta method is given by

$$(2.17) \qquad \begin{aligned} u^{(1)} &= u^n + \Delta t\, L(u^n) \\ u^{n+1} &= \tfrac{1}{2}u^n + \tfrac{1}{2}u^{(1)} + \tfrac{1}{2}\Delta t\, L(u^{(1)}) \end{aligned}$$

The optimal third-order TVD Runge-Kutta method is given by

$$(2.18) \qquad \begin{aligned} u^{(1)} &= u^n + \Delta t\, L(u^n) \\ u^{(2)} &= \tfrac{3}{4}u^n + \tfrac{1}{4}u^{(1)} + \tfrac{1}{4}\Delta t\, L(u^{(1)}) \\ u^{n+1} &= \tfrac{1}{3}u^n + \tfrac{2}{3}u^{(2)} + \tfrac{2}{3}\Delta t\, L(u^{(2)}) \end{aligned}$$

In [2], it has been shown that, even with a very nice second-order TVD spatial discretization, if the time discretization is by a non-TVD but linearly stable Runge-Kutta method, the result may be oscillatory. Thus it would always be safer to use TVD Runge-Kutta methods for hyperbolic problems.

The description of the scheme is complete when a proper non-oscillatory flux (2.5) is chosen. In the next section we review the possible upwind and central fluxes which can be used.

3. Numerical fluxes

The initial value problem (IVP) for the one-dimensional scalar hyperbolic conservation law is considered, namely

$$(3.1a) \qquad u_t + f(u)_x = 0, \quad -\infty < x < \infty, \quad t \geq 0$$

$$(3.1b) \qquad u(x,0) = u_0(x)$$

where f is the flux and $a(u) = \partial f/\partial u$ is the wave (characteristic) speed.

The general numerical scheme to solve (3.1) takes the form

$$(3.2) \qquad u_j^{n+1} = u_j^n - \lambda \left[f_{j+\frac{1}{2}} - f_{j+\frac{1}{2}} \right]$$

where $f_{j+\frac{1}{2}}$ is the numerical flux. The description of the scheme is complete when a proper non-oscillatory flux (3.2) is chosen. In this section we review the possible upwind and central fluxes which can be used.

3.1. Upwind fluxes

Upwind fluxes utilise information on local wave propagation explicitly.
The numerical flux (3.2) is written in the form

$$f_{j+\frac{1}{2}} = \frac{1}{\Delta t} \int\limits_{t^n}^{t^{n+1}} f\left(u(x_{j+\frac{1}{2}}, \tau)\right) d\tau$$

Here, it remains to recover the point-values, $u(x_{j+\frac{1}{2}}, \tau)$, $t^n \leq \tau \leq t^{n+1}$,
in terms of their known cell averages $\{u_j^n\}$, and to this end we proceed in two
steps:

-First, the reconstruction: we recover the point-wise values of $u(., \tau)$ at
$\tau = t^n$, by reconstruction of a piecewise polynomial approximation

(3.3) $u(x, t^n) = P_j(x)$

-Second, the evolutions $u(x_{j+\frac{1}{2}}, \tau \geq t^n)$ are determined as the solutions of
the Generalized Riemann problems (GRP)

(3.4) $u_t + f(u)_x = 0, \quad t \geq t^n, \quad u(x, t^n) = \begin{cases} P_j(x), & x < x_{j+\frac{1}{2}} \\ P_{j+1}(x), & x > x_{j+\frac{1}{2}} \end{cases}$

The solution of (3.4) is composed of a family of nonlinear waves, left-going
and right-going waves. An exact Riemann solver or at least an approximate
one is used to distribute these nonlinear waves between the two neighbouring
cells I_j and I_{j+1}. The original Godunov scheme is based on piecewise constant
reconstruction $P_j(x) = u_j$ and $P_{j+1}(x) = u_{j+1}$, followed by an exact Riemann
solver. This results in a first order accurate upwind method, which is the fore-
runner for all other upwind schemes. A second order extension was introduced
by Van Leer [12]: his MUSCL scheme reconstructs a piecewise linear approxima-
tion $u(x, t^n) = P_j(x)$ with linear piecewise of the form $P_j(x) = u_j^n + u_j'(\frac{x-x_j}{\Delta x})$.
Here u_j' is a limited slope. The ENO schemes by Harten et al. [4] and WENO
schemes [5] offer higher-order upwind schemes.

3.2. Central fluxes

Probably, the most well known central flux is the LxF flux given by

(3.5) $f_{j+\frac{1}{2}}^{LF}\left(u_{j+\frac{1}{2}}^L, u_{j+\frac{1}{2}}^R\right) = \frac{1}{2}(f_{j+\frac{1}{2}}^L + f_{j+\frac{1}{2}}^R) - \frac{1}{2}\frac{\Delta x}{\Delta t}(u_{j+\frac{1}{2}}^R - u_{j+\frac{1}{2}}^L)$

the LxF flux is commonly used in the design of some high-order methods. In the
limiting case of piecewise constant data $u_{j+\frac{1}{2}}^L = u_j^n$, $u_{j+\frac{1}{2}}^R = u_{j+1}$, this flux leads
to a monotone first-order accuracy fully discrete scheme. Nessyahu and Tadmor
introduced in [7] a second-order extension (NT) along these lines, using the
piecewise linear MUSCL reconstructions results a non-oscillatory, second-order
scheme in which the excessive smearing typical to the first-order LxF central

scheme is compensated by the second order accurate MUSCL reconstruction. At the same time, the NT second-order central scheme has the advantage on the corresponding upwind schemes, in that no Riemann solvers are required. In [6], Liu and Tadmor introduced a third-order central scheme by using the piecewise quadratic MUSCL reconstructions with the same framework of NT scheme. In [1], the third and fourth-order central schemes are presented. These schemes can be viewed as extensions of second-order NT scheme, where the ENO reconstruction is used instead of MUSCL reconstructions.

3.3. Third-order fully discrete TVD scheme

In this section a third-order explicit TVD scheme presented in [13] is reviewed.

The third-order conservation TVD numerical scheme introduced in [13] has the form (for constant a)

$$(3.6) \qquad u_j^{n+1} = u_j^n - \lambda \left[f_{j+\frac{1}{2}} - f_{j+\frac{1}{2}} \right]$$

with the numerical flux

$$f_{j+\frac{1}{2}} = \frac{1}{2} \left(au_j + au_{j+1} \right) - \frac{1}{2} |a| \, \Delta_{j+\frac{1}{2}} u +$$

$$(3.7) \qquad + |a| \left\{ A_0 \Delta_{j+\frac{1}{2}} u + A_1 \Delta_{j+L+\frac{1}{2}} u + A_2 \Delta_{j+M+\frac{1}{2}} u \right\}$$

where

$$(3.8) \qquad A_0 = \frac{1}{2} - \frac{|c|}{4}, \quad A_1 = -\frac{|c|}{8} - \frac{c^2}{8}, \quad A_2 = -\frac{|c|}{8} + \frac{c^2}{8}$$

$L = -1, M = 1$ for $c > 0$ and $L = 1, M = -1$ for $c < 0$

Where $c = \lambda a$ is the Courant number and $\Delta_{j+\frac{1}{2}} u = u_{j+1} - u_j$.

This scheme, being a third-order accurate scheme, is not TVD. It can be made TVD by replacing (3.7) with the more general form

$$(3.9) \qquad \begin{array}{l} f_{j+\frac{1}{2}} = \frac{1}{2} \left(au_j + au_{j+1} \right) - \frac{1}{2} |a| \, \Delta_{j+\frac{1}{2}} u + \\ |a| \left\{ A_0 \Delta_{j+\frac{1}{2}} u + A_1 \Delta_{j+L+\frac{1}{2}} u \right\} \varphi_j + |a| \ A_2 \Delta_{j+M+\frac{1}{2}} u \phi_{j+M} \end{array}$$

where ϕ_j and ϕ_{j+M} are flux limiter functions.

Theorem 3.1 *Scheme (3.6) with (3.9) is TVD for $|c| \leq 1$ if the limiter function is determined by*

$$(3.10a) \qquad \phi_j = \begin{cases} \frac{(1-|c|)\theta_j}{\eta(A_1\theta_j + A_0 - A_2)} & \text{for } 0 \leq \theta_j \leq \theta^L \\ 1 & \text{for } \theta^L \leq \theta_j \leq \theta^R \\ \frac{1-|c|+\eta A_2 \phi_{j+M}/\theta_j^*}{\eta(A_1\theta_j + A_0)} & \text{for } \theta_j > \theta^R \\ 0 & \text{for } \theta_j < 0 \end{cases}$$

$$(3.10b) \qquad \phi_{j+M} = \begin{cases} \eta\theta_{j+M} & for\ 0 \le \theta_{j+M} < 0.5 \\ 1 & for\ \theta_{j+M} > 0.5 \\ 0 & for\ \theta_j = 0 \end{cases}$$

where

$$\theta^L = \frac{\eta\ (A_0 - A_2)}{1 - |c| - \eta\ A_1}, \qquad \theta^R = \frac{1 - |c| - \eta\ (A_0 - A_2\phi_{j+M}/\theta_j^*)}{\eta\ A_1}$$

where θ_j is called the local flow parameter and is defined by

$$(3.10c) \qquad \theta_j = \frac{\Delta_{j+L+\frac{1}{2}}u}{\Delta_{j+\frac{1}{2}}u}$$

and θ_j^* is called the upwind-downward flow parameter and is given by

$$(3.10d) \qquad \theta_j^* = \frac{\Delta_{j+L+\frac{1}{2}}u}{\Delta_{j+M+\frac{1}{2}}u}$$

and η is defined by

$$(3.10e) \qquad \eta = \begin{cases} 1 - |c| & for\ 0 \le |c| < \frac{1}{2} \\ |c| & for\ \frac{1}{2} \le |c| \le 1 \end{cases}$$

Proof. see [8] and [13]. $\qquad\qquad\qquad\qquad\qquad\qquad\qquad\qquad\qquad\qquad\qquad\qquad\qquad\square$

For nonlinear scalar problems $a = a(u)$, we define the wave speed

$$(3.11) \qquad a_{j+\frac{1}{2}} = \begin{cases} \frac{\Delta_{j+\frac{1}{2}}f}{\Delta_{j+\frac{1}{2}}u} & \Delta_{j+\frac{1}{2}}u \ne 0 \\ \left.\frac{\partial f}{\partial u}\right|_{u_j} & \Delta_{j+\frac{1}{2}}u = 0 \end{cases}$$

Now we redefine θ_j in (3.10c) as

$$(3.12) \qquad \theta_j = \frac{\left|a_{j+L+\frac{1}{2}}\right|\Delta_{j+L+\frac{1}{2}}u}{\left|a_{j+\frac{1}{2}}\right|\Delta_{j+\frac{1}{2}}u}$$

Here $c_{j+\frac{1}{2}} = \frac{\Delta t}{\Delta x}\ a_{j+\frac{1}{2}}$ The numerical flux (3.9) takes the form

$$
\begin{aligned}
f_{j+\frac{1}{2}} \quad = \quad & \frac{1}{2}\ (f_j + f_{j+1}) - \frac{1}{2}\left|a_{j+\frac{1}{2}}\right|\Delta_{j+\frac{1}{2}}u \\
& + \left|a_{j+\frac{1}{2}}\right|\ \left\{ A_0\Delta_{j+\frac{1}{2}}u + A_1\Delta_{j+L+\frac{1}{2}}u \right\}\ \varphi_j \\
(3.13) \qquad & + \left|a_{j+\frac{1}{2}}\right|A_2\Delta_{j+M+\frac{1}{2}}u\phi_{j+M}
\end{aligned}
$$

The flux limiter becomes the same (3.9) with replacing c by $a_{j+\frac{1}{2}}$.

4. Description of the method

In this section we combine the central framework which was overviewed in section 3 with the WENO reconstruction of section 2. We notice from section (3.2) that most of numerical methods, that only lower (first-order) monotone fluxes are used as a building block for the construction of higher order schemes. Here we propose to use the third-order TVD flux as a building block in high order WENO schemes with TVD Runge-Kutta method for time stepping.

The derivation of the resulting scheme is straightforward and is summarized in the following algorithm, which applies to the scalar case:

Given the cell averages u_j^n, at time t^n, compute the cell averages at the next time step u_j^{n+1} as follows:

1) We obtain the $(2k-1)$-th order WENO approximations to the function u (x) at the cell boundaries, denoted by $u_{j+\frac{1}{2}}^L, u_{j+\frac{1}{2}}^R$ in the following way:

a) obtain k reconstructed values $u_{j+\frac{1}{2}}^{(r)}$, of k-th order accuracy, in (2.7) based on the stencils (2.6), for $r = 0, \ldots, k-1$

b) find the constants d_r such that (2.10) is valid;

c) find the smooth indicators β_r, for all $r = 0, \ldots, k-1$, from (2.14) or (2.15);

d) form the weights w_r from (2.12);

e) find the $(2k-1)$-th order reconstructions $u_{j+\frac{1}{2}}^L = P_j(x_{j+\frac{1}{2}})$, $u_{j+\frac{1}{2}}^R = P_{j+1}(x_{j+\frac{1}{2}})$, where $P_j(x_{j+\frac{1}{2}})$ is defined in equation (2.9).

2) Compute the third-order TVD flux (3.9) with $\Delta_{j+\frac{1}{2}} u = u_{j+\frac{1}{2}}^R - u_{j+\frac{1}{2}}^L$, for all j;

3) Form the scheme (2.3)

4) Using the third-order TVD Runge-Kutta method (2.17) or (2.18), compute u_j^{n+1} .

We end this section sketching the algorithm for the case of $m \times m$ systems of conservation laws

$$U_t + F(U)_x = 0,$$

where $U = (u^1, ... u^m)$ is a vector of m components, the conserved variables and $F(U) = (f(u^1), ..., f(u^m))$ is the corresponding vector fluxes.

Given the cell averages U_j^n, at time t^n, compute the cell averages at the next time step U_j^{n+1} as follows:

1) Compute the interpolant polynomial $P_j(x)$ applying step 1 of the last algorithm at each component of the vector U_j^n. Note that the coefficients of the interpolant are now m-component vectors. For the computation of smooth indicators β_r, one can apply formulas (2.14) or (2.15), obtaining different smooth indicators for each component.

2) Compute left and right extrapolations vector values $U_{j+\frac{1}{2}}^L = P_j(x_{j+\frac{1}{2}})$, $U_{j+\frac{1}{2}}^R = P_{j+1}(x_{j+\frac{1}{2}})$.

3) Compute the vector flux $F_{j+\frac{1}{2}}(U_j^n)$ by applying the reconstruction procedure (3.9) at each component of $F(U)$.

4) Apply steps 3 and 4 of the scalar algorithm to each component of conservation law, to get U_j^{n+1} .

5. Numerical Results

In this section, we test our new scheme proposed here. We first compare our semi-discrete finite volume scheme with the original Toro scheme with second-order flux [10] and compare the results of this scheme with those of other state of the art high-order shock capturing methods, such as central ENO scheme [1]. Here we use, throughout, the finite volume scheme, presented in section 4, with the fifth-order WENO reconstruction and the time evolution is computed by the third-order TVD Runge-Kutta method.

An important issue is the choice of test problems. We would like to emphasise here the importance of using really long-time evolution problems with solutions consisting of discontinuities and smooth parts.

We compare the following schemes:

1- TORO: it is Toro scheme with the second-order TVD flux,

2- ENO3: it is the third order central ENO scheme presented in [1].

3- WENTVD: it is our scheme presented in section 4.

5.1. Scalar equations

We study the performance of our scheme by applying it to the following problems:

Example 1

We solve the transport equation

$$(5.1) \qquad\qquad u_t + u_x = 0, \qquad x \in [-1, 1]$$

subjected to periodic initial data

$$(5.2) \qquad\qquad u(x, 0) = \sin(\pi x)$$

This test is used to check the convergence rate at large times. For each scheme we select a value of λ that satisfies the linear stability condition. Scheme ENO3 has $\lambda = 0.386$ and the others have $\lambda = 0.8$. The results obtained for example 1, at time $t = 10$, are shown in Tables 1 and 2. It can be seen that WENTVD scheme is the most accurate and it is less expensive because it enjoys a less restrictive CFL condition ($\lambda = 0.8$ versus $\lambda = 0.386$). Comparing the magnitudes of the errors with the results obtained with ENO3 and TVD3, we note that our new WENTVD scheme yields smaller errors than the others.

Table 1

N	TORO		ENO3		WENTVD	
	L^1 error	L^1 order	L^1 error	L^1 order	L^1 error	L^1 order
20	2.9210E-1		0.1387E-1		0.8872E-2	
40	4.5831E-2	2.67	0.1483E-2	3.2252	0.6091E-3	3.864
80	1.1149E-2	2.04	0.1799E-3	3.0436	0.4309E-4	3.820
160	2.3602E-3	2.24	0.2229E-4	3.0125	0.3633E-5	3.568
320	5.2731E-4	2.16	0.2774E-5	3.0065	0.3947E-6	3.202
640	1.2491E-4	2.08	0.3463E-6	3.0020	0.4766E-7	3.045

Table 2

N	TORO		ENO3		WENTVD	
	L^∞ error	L^∞ order	L^∞ error	L^∞ order	L^∞ error	L^∞ order
20	3.1509E-1		0.1553E-1		0.1069E-1	
40	9.9631E-2	1.66	0.1921E-2	3.0151	0.1269E-2	3.0745
80	3.7040E-2	1.43	0.2293E-3	3.0666	0.1382E-3	3.2009
160	1.2631E-2	1.55	0.2710E-4	3.0813	0.1541E-4	3.1623
320	4.4631E-3	1.50	0.3211E-5	3.0775	0.1738E-5	3.1492
640	1.6903E-3	1.40	0.3817E-6	3.0721	0.1944E-6	3.1611

Example 2.

We now consider the equation (5.1) with the initial condition [5]

(5.3)
$$
u(x,0) = \begin{cases} \frac{1}{6}[G(x,z-\delta) + G(x,z+\delta) + 4G(x,z)], & -0.8 \le x \le -0.6 \\ 1, & -0.4 \le x \le -0.2 \\ 1 - |10(x-0.1)|, & 0 \le x \le 0.2 \\ \frac{1}{6}[F(x,a-\delta) + F(x,a+\delta) + 4F(x,a)], & 0.4 \le x \le 0.6 \\ 0, & \text{otherwise} \end{cases}
$$

with periodic boundary condition on [-1,1].

Where $G(x,z) = \exp(-\beta(x-z)^2)$, $F(x,a) = \{\max(1 - \alpha^2(x-a)^2\}^{\frac{1}{2}}$.

The constants are taken as $a = 0.5$, $z = -0.7$, $\delta = 0.005$, $\alpha = 10$ and $\beta = (\log 2)/36\delta^2$.

This initial condition consists of several shapes which are difficult for numerical methods to resolve correctly. Some of these shapes are not smooth and the others are smooth but very sharp.

Figure 1 shows the results of TVD3 and WENTVD schemes for $t = 10$ on the mesh of 200 cells, $\lambda = 0.8$. The full line corresponds to the exact solution and symbols correspond to the numerical solution. We observe that the TVD3 scheme produces good results while the new scheme WENTVD is significantly more accurate. As expected, the WENTVD scheme produces the most accurate results for all parts, including the square pulse. The resolution of the contact
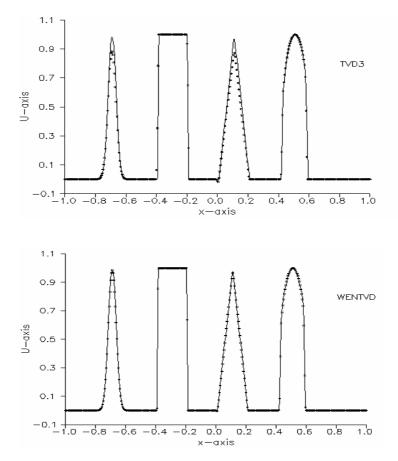
Figure 1: Solution of example 2 at $t = 10$, by TVD3 scheme (top) and WENTVD scheme (bottom)

discontinuities present in the square wave seems better than the analogous results obtained by ENO and WENO schemes by Jiang and Shu (see [5]).

Example 3. (Burger equation)

$$(5.4a) \qquad u_t + (\frac{1}{2}u^2)_x = 0, \qquad x \in [0,1]$$

with smooth periodic data

$$(5.4b) \qquad u(x,0) = \sin(2\pi x), \quad u(0) = u(1)$$

Figures 2 and 3 show the results at $t = 0.15$ (before shock formation) and $t = 0.32$ (after shock formation) respectively. Note that the shock develops at $t = \frac{1}{2\pi} \approx 0.16$

Note that the original scheme TVD3 gives sharp resolution discontinuity while the results obtained by WENTVD are almost indistinguishable from the exact solutions.
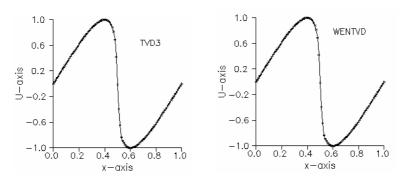

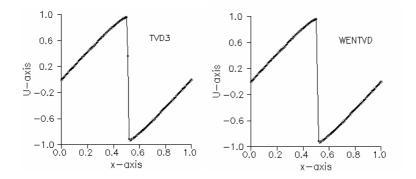Figure 2: Solution of example 3 at $t = 0.32$, by TVD3 scheme (left) and WENTVD scheme (right)

Figure 3: Solution of example 3 at $t = 0.32$ by TVD3 scheme (left) and WENTVD scheme (right)

5.2. Systems of equations

We apply our new scheme to the system of Euler equations of gas dynamics

$$(5.5) \qquad U_t + F(U)_x = 0,$$

where $U = (\rho, \rho u, E)^T$ and $F(U) = (\rho u, \rho u^2 + P, u(E + P))^T$, where ρ is the density, u is the velocity, P is the pressure, $E = \frac{1}{2}\rho u^2 + \frac{P}{(\gamma-1)}$ is the total energy and γ is the ratio of specific heats, taken as 1.4 here.

Example 4.

The first problem is the shock tube problem [5]. The computational domain is taken as the unit interval [0,1] divided into 100 cells.

Initial conditions consist of two states, left (L) and right (R)

(5.6) $(\rho_L, u_L, P_L) = (1, 0, 1)$ and $(\rho_R, u_R, P_R) = (0.125, 0, 0.1)$

separated by a discontinuity at $x = 0.5$. Output is taken at time $t = 0.2$. Plots of density, velocity and pressure taken for $\lambda = 0.8$ with TVD3 and WENTVD schemes are shown in Figure 4. The solid line represents the exact solution and symbols represent the numerical solution.
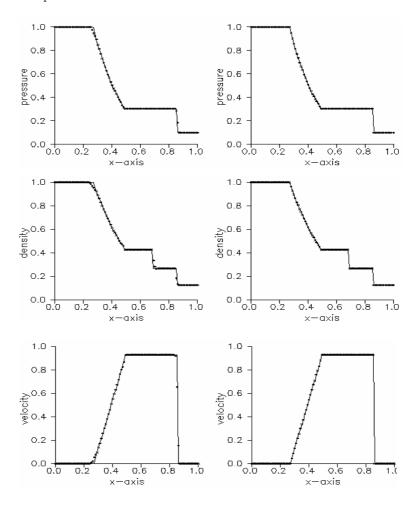

Figure 4: Solution of Euler equations for example 4 via TVD3 (left) and WENTVD (right)

It is clear that the results obtained by TVD3 scheme are satisfactory for both smooth parts and shocks, while the results obtained by WENTVD scheme are almost indistinguishable from the exact solutions.

Example 5. (Double blast waves)

The second initial value problem here is that introduced by Woodward and Colella [11]. Initial condition consists of three states

$$(5.9) \qquad U(x,0) = \begin{cases} (\rho_L, u_L, P_L) = (1,0,1000), & x < 0.1 \\ (\rho_M, u_M, P_M) = (1,0,0.01), & 0.1 < x < 0.9 \\ (\rho_R, u_R, P_R) = (1,0,100), & x > 0.9 \end{cases}$$
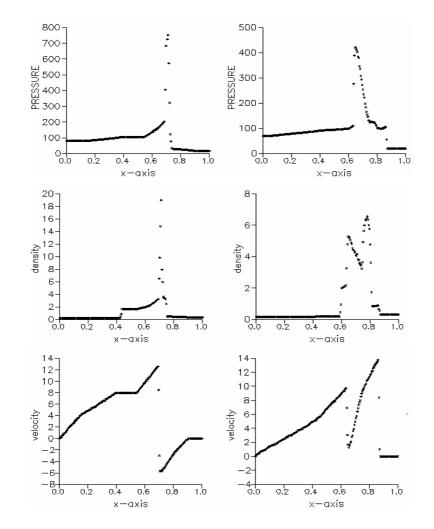

Figure 5: Solution of example 5 by WENTVD scheme at t = 0.28 (left) and t = 0.38 (right)

Boundary conditions are reflective. The solution of this problem contains the propagation of strong shock waves into low pressure regions, the collision of

strong shock waves and interaction of shock waves and rarefactions, and is thus a good test of the scheme. We take $\lambda = 0.8$ with 200 cells. Figure 5 shows the results obtained by the WENTVD scheme at $t = .028$ and $t = .038$. There is no exact solution for this case.

Comparing with the results shown (reference solution) in [11], it is remarkable that the WENTVD scheme is able to obtain such sharp resolution of the complex double blast problem.

References

[1] Bianco, F., Puppo, G., Russo, G., High-order central schemes for hyperbolic systems of conservation laws. SIAM J. Sci. Comput. 21 (1999), 294-322.

[2] Gotlieb, S., Shu, C. W., Total variation diminishing Runge-Kutta schemes. Math. Comp. 67 (1998), 73-85.

[3] Harten, A., High resolution schemes for hyperbolic conservation laws. J. Comput. Phys. 49 (1983), 357-393.

[4] Harten, A., Enqueist,B., Osher, S., Chakravarthy, S. R., Uniformly high-order accurate essentially non oscillatory schemes. J. Comput. Phys. 71 (1987), 231-303.

[5] Jiang, G. S., Shu, C. W., Efficient implementation of Weighted ENO schemes. J. Comut. Phys. 126 (1996), 202-228.

[6] Liu X. D., Tadmor, E., Third order non-oscillatory central scheme for hyperbolic conservation laws. J. Numer. Math. 79 (1998), 397-425.

[7] Nessyahu, H., Tadmor, E., Non oscillatory central differencing for hyperbolic conservation laws. J. Comput. Phys. 87 (1990), 408-463.

[8] Shi, J., Toro, E. F., Fully discrete high resolution schemes for hyperbolic conservation laws. Int. J. Num. Method Fluids 23 (1996) 241-269.

[9] Shu C. W., Essentially non-oscillatory and weighted ENO for hyperbolic conservation laws. NASA/CR 97-206253, ICASE Report No. 97-65 (1997)

[10] Titarev, V. A., Toro, E. F., ENO and WENO schemes based on upwind and centred TVD fluxes. J. Computers and Fluids 34 (2005), 705-720.

[11] Woodward, P., Colella, P., The numerical solution of two-dimensional fluid flow with strong waves. J. Comput. Phys. 54 (1984), 115-173.

[12] VanLeer, B., Towards the ultimate conservative difference scheme, V. A second order sequel to Godunovs method. J. Comput. Phys. 32 (1979), 101-136.

[13] Zahran, Y. H., Third order TVD scheme for hyperbolic conservation laws. Bulletin of the Belgian Mathematical Society, in press.